SCIENCE CHINA
Information Sciences

• RESEARCH PAPERS •
Special Focus

March 2011 Vol. 54 No. 3: 482–497
doi: 10.1007/s11432-011-4186-y

Adaptive recurrent-functional-link-network control for hypersonic vehicles with atmospheric disturbances

DU YanLi[1]*, WU QingXian[2], JIANG ChangSheng[2] & XUE YaLi[2]

[1]*College of Astronautics, Nanjing University of Aeronautics and Astronautics, Nanjing* 210016*, China;*
[2]*College of Automation Engineering, Nanjing University of Aeronautics and Astronautics, Nanjing* 210016*, China*

Received July 2, 2010; accepted December 14, 2010

Abstract The controller design for a near-space hypersonic vehicle (NHV) is challenging due to its plant uncertainties and sensitivity to atmospheric disturbances such as gusts and turbulence. This paper first derives 12 states equations of NHVs subjected to variable wind field, and presents a novel recurrent neural network (RNN) control method for restraining atmospheric disturbances. The method devises a new B-spline recurrent functional link network (BRFLN) and combines it with the nonlinear generalized predictive control (NGPC) algorithm. Moreover, the proportional-derivative (PD) correction BRFLN is proposed to approximate atmospheric disturbances in flight. The weights of BRFLN are online tuned by the adaptive law based on Lyapunov stability theorem. Finally, simulation results show a satisfactory performance for the attitude tracking of the NHV in the mesosphere, and also illustrate the controller's robustness to wind turbulence.

Keywords near-space hypersonic vehicle, atmospheric disturbances, nonlinear predictive control, adaptive control, B-spline recurrent functional link network

Citation Du Y L, Wu Q X, Jiang C S, et al. Adaptive recurrent-functional-link-network control for hypersonic vehicles with atmospheric disturbances. Sci China Inf Sci, 2011, 54: 482–497, doi: 10.1007/s11432-011-4186-y

1 Introduction

There are several critical problems facing the controller design of near-space hypersonic vehicles (NHVs). Two of them make precise attitude control of NHVs very challenging. One is the high nonlinearity of system dynamics and the strong coupling between the airframe, propulsion and control system; the other is that we have to deal with heavy uncertainties including aerodynamic parameter variations, aeroelastic effects, propulsion system perturbation, atmospheric disturbances, etc.

Recently, many researchers utilized different nonlinear control strategy to handle model nonlinearity to the first problem [1–3]. As for the second, lots of literatures presented adaptive or robust longitudinal control laws under aerodynamic parameter variations [3, 4]. In addition, Buschek [5] designed fixed-order μ controllers considering the aeroelastic deformation, and Wilcox [6] presented a robust output feedback controller for capturing aerothermoelastic effects. Except for above researches, the authors of this paper proposed partially-feedback-functional-link-network (PFFLN) adaptive control method [7],

*Corresponding author (email: duylnuaa@yahoo.cn)

and applied it to an NHV in the presence of fast-loop moment disturbance induced by propulsion system perturbation. However, as far as we know, no literature has discussed in detail the NHV controller design with atmospheric disturbances which involve gusts, turbulence and wind shear. The major difficulty lies in the derivation of NHV's nonlinear model under variable wind field and the lack of atmospheric data in the near space (20–100 km above the earch). Based on the analysis of near space wind model (newly published in [8]), this paper derives 6 degree-of-freedom and 12 states nonlinear equations of NHVs subjected to wind field. In order to handle these wind disturbances, we also propose a new nonlinear adaptive controller to improve the attitude tracking performance.

The control strategy mainly consists of a continuous-time nonlinear generalized predictive control (NGPC) law and a B-spline recurrent-functional-link-network (BRFLN) control adjustment. The nominal NGPC law [9] can avoid the online computation and it is an effective algorithm for fast time-varying systems, especially for NHVs' control system. Hence, the NGPC is used to stabilize the dynamics of an NHV. The functional link network (FLN) [10] is a single-layer NN with functionally mapped inputs. It has simpler structure and higher computation speed than a multi-layer perceptron (MLP) [11, 12]. The BRFLN, presented in this paper, not only possesses characteristics as those of the FLN, but also is capable of learning dynamical high-order nonlinear functions. Moreover, we first introduce the n-order B-spline functions in this network. As we know, atmospheric disturbances are dynamically changeable, so RNNs will be more suitable for their approximation than static NNs. Because the BRFLN has simpler structure than common RNNs with hidden layers, it may be relatively easy for us to implement the control algorithms of NHVs. Accordingly, the BRFLN acts as an aid to the NGPC law for compensating disturbances/uncertainties of the fast-loop attitude system, and the proportional-derivative (PD) correction BRFLN is used for learning disturbances/uncertainties of the slow-loop attitude system. The feedforward and feedback weights of the BRFLN are online tuned by the adaptive law based on Lyapunov stability theorem. A robust control (RC) item with adaptive gain is also proposed to counteract errors between the BRFLN and disturbances. In summary, the presented BRFLN-based NGPC method does not require the knowledge about uncertainty bounds, and it is an effective algorithm to resolve NHV control problems arising out of atmospheric disturbances.

The paper is organized as follows: in section 2, we derive 12 states nonlinear equations of NHVs subjected to variable wind field. Section 3 discusses the design of the BRFLN-based NGPC method for an NHV. In section 4, we give the stability analysis of the closed-loop attitude system. Finally, simulation results of the airflow angles and angular rates control systems are shown followed by the conclusions.

2 The NHV model with atmospheric disturbances

NHVs fly in the upper stratosphere and the whole mesosphere which is often called "high altitude troposphere". Because atmospheric convective motions are strong in the mesosphere, the wind shear and turbulence frequently occur there [8]. Hence, the effects that near-space wind field produces cannot be ignored. The NHV model comes from a winged-cone configuration vehicle [13]. Figure 1 shows the variables relationship of the NHV.

The wind vector $\boldsymbol{V}_W = [u_{Wb}, v_{Wb}, w_{Wb}]^{\mathrm{T}}$, the airspeed vector $\boldsymbol{V}_A = [u_{Ab}, v_{Ab}, w_{Ab}]^{\mathrm{T}}$ and the groundspeed vector $\boldsymbol{V}_K = [u_{Kb}, v_{Kb}, w_{Kb}]^{\mathrm{T}}$ satisfy the triangular relationship as Figure 1 shows, that is, $\boldsymbol{V}_K = \boldsymbol{V}_A + \boldsymbol{V}_W$. D, Y, L and G denote the resistance force, the side force, the lift force and the gravity. Considering the low efficiency of aerodynamic control surfaces in the near-space, we employ motor thrust vector $\boldsymbol{T} = [T_{xb}, T_{yb}, T_{zb}]^{\mathrm{T}}$. All variables' subscripts, the lowercase letters g, b, a and k mean that these vectors are expressed in the ground, the body, the airflow and the path axis coordinate system. Hence, T_{gb}, T_{ba}, T_{ag} and T_{gk} are transformation matrices between two different coordinate systems [14]. We will derive 12 states equations including angle of attack α, angle of sideslip β and angle of bank μ, because the precise control of these angles is essential to the control system.

Firstly, from $\boldsymbol{V}_K = \boldsymbol{V}_A + \boldsymbol{V}_W$, we have the NHV position equation as follows:

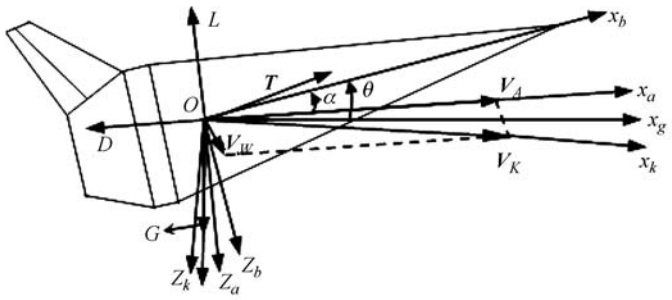

Figure 1 The variables relationship of the NHV longitudinal model.

$$\begin{aligned}\begin{bmatrix}\dot{x}_g\\ \dot{y}_g\\ \dot{z}_g\end{bmatrix} &= \begin{bmatrix}u_{Kg}\\ v_{Kg}\\ w_{Kg}\end{bmatrix} = T_{gb}\begin{bmatrix}u_{Kb}\\ v_{Kb}\\ w_{Kb}\end{bmatrix} = T_{gb}\left\{\begin{bmatrix}u_{Ab}\\ v_{Ab}\\ w_{Ab}\end{bmatrix} + \begin{bmatrix}u_{Wb}\\ v_{Wb}\\ w_{Wb}\end{bmatrix}\right\}\\ &= T_{gb}\left\{T_{ba}\begin{bmatrix}V_A\\ 0\\ 0\end{bmatrix} + T_{bg}\begin{bmatrix}u_{Wg}\\ v_{Wg}\\ w_{Wg}\end{bmatrix}\right\},\end{aligned} \tag{1}$$

where $T_{gb}\cdot T_{ba} = T_{ga}$, and $T_{gb}\cdot T_{bg}$ equals to unit matrix. So we get

$$\begin{bmatrix}\dot{x}_g\\ \dot{y}_g\\ \dot{z}_g\end{bmatrix} = \begin{bmatrix}V_A\cos\gamma_a\cos\chi_a\\ V_A\cos\gamma_a\sin\chi_a\\ -V_A\sin\gamma_a\end{bmatrix} + \begin{bmatrix}u_{Wg}\\ v_{Wg}\\ w_{Wg}\end{bmatrix}, \tag{2}$$

where $[V_A, 0, 0]^{\mathrm{T}}$ is the expression of $\boldsymbol{V}_A$ in the airflow axis system and V_A is the module value of $\boldsymbol{V}_A$. γ_a and χ_a are the path angle and the heading angle.

Secondly, using the kinetics equation of NHVs, i.e. $m\cdot d\boldsymbol{V}_K/dt = \Sigma F$, and treating the body axis system as the reference frame, we obtain

$$\begin{bmatrix}\dot{u}_{Kb}\\ \dot{v}_{Kb}\\ \dot{w}_{Kb}\end{bmatrix} + \begin{vmatrix} i & j & k\\ p_K & q_K & r_K\\ u_{Kb} & v_{Kb} & w_{Kb}\end{vmatrix} = \frac{1}{m}\left\{\begin{bmatrix}T_{xb}\\ T_{yb}\\ T_{zb}\end{bmatrix} + T_{ba}\begin{bmatrix}-D\\ Y\\ -L\end{bmatrix} + T_{bg}\begin{bmatrix}0\\ 0\\ mg\end{bmatrix}\right\}, \tag{3}$$

where $\omega = [p_K, q_K, r_K]^{\mathrm{T}}$ is the NHV angular rate vector with respect to the ground and expressed in the body axis system. In addition, m is the NHV mass. The application of (1) yields

$$\begin{aligned}&\dot{T}_{ba}\begin{bmatrix}V_A\\ 0\\ 0\end{bmatrix} + T_{ba}\begin{bmatrix}\dot{V}_A\\ 0\\ 0\end{bmatrix} + \dot{T}_{bg}\begin{bmatrix}u_{Wg}\\ v_{Wg}\\ w_{Wg}\end{bmatrix} + T_{bg}\begin{bmatrix}\dot{u}_{Wg}\\ \dot{v}_{Wg}\\ \dot{w}_{Wg}\end{bmatrix}\\ &= \frac{1}{m}\left\{\begin{bmatrix}T_{xb}\\ T_{yb}\\ T_{zb}\end{bmatrix} + T_{ba}\begin{bmatrix}-D\\ Y\\ -L\end{bmatrix} + T_{bg}\begin{bmatrix}0\\ 0\\ mg\end{bmatrix}\right\} - \begin{bmatrix}0 & -r_K & q_K\\ r_K & 0 & -p_K\\ -q_K & p_K & 0\end{bmatrix}\begin{bmatrix}u_{Kb}\\ v_{Kb}\\ w_{Kb}\end{bmatrix},\end{aligned} \tag{4}$$

where T_{bg} is the function matrix of Euler angles ϕ, θ and ψ. These angles are not the controlled variables in this paper, so $\dot{T}_{bg} = 0$. Multiplying the two sides of (4) by T_{ab}, we get

$$T_{ab}\dot{T}_{ba}\begin{bmatrix}V_A\\ 0\\ 0\end{bmatrix} + \begin{bmatrix}\dot{V}_A\\ 0\\ 0\end{bmatrix} + T_{ag}\begin{bmatrix}\dot{u}_{Wg}\\ \dot{v}_{Wg}\\ \dot{w}_{Wg}\end{bmatrix}$$

$$= \frac{1}{m}\left\{\begin{bmatrix} -D \\ Y \\ -L \end{bmatrix} + T_{ab}\begin{bmatrix} T_{xb} \\ T_{yb} \\ T_{zb} \end{bmatrix} + T_{ag}\begin{bmatrix} 0 \\ 0 \\ mg \end{bmatrix}\right\}$$
$$- T_{ab}\begin{bmatrix} 0 & -r_K & q_K \\ r_K & 0 & -p_K \\ -q_K & p_K & 0 \end{bmatrix}\left\{T_{ba}\begin{bmatrix} V_A \\ 0 \\ 0 \end{bmatrix} + \begin{bmatrix} u_{Wb} \\ v_{Wb} \\ w_{Wb} \end{bmatrix}\right\}. \quad (5)$$

We ignore the angular rate effect which $[u_{wb}, v_{wb}, w_{wb}]^{\mathrm{T}}$ brings about because of its tiny influence. Then,

$$\begin{bmatrix} \dot{V}_A \\ V_A \cdot \dot{\beta} \\ (V_A \cos\beta)\cdot\dot{\alpha} \end{bmatrix} = \frac{1}{m}\left\{\begin{bmatrix} -D \\ Y \\ -L \end{bmatrix} + T_{ab}\begin{bmatrix} T_{xb} \\ T_{yb} \\ T_{zb} \end{bmatrix} + T_{ag}\begin{bmatrix} 0 \\ 0 \\ mg \end{bmatrix}\right\}$$
$$- \begin{bmatrix} 0 \\ r_K V_A \cos\alpha - p_K V_A \sin\alpha \\ r_K V_A \sin\beta\sin\alpha + p_K V_A \sin\beta\cos\alpha - q_K V_A \cos\beta \end{bmatrix} - T_{ag}\begin{bmatrix} \dot{u}_{Wg} \\ \dot{v}_{Wg} \\ \dot{w}_{Wg} \end{bmatrix}. \quad (6)$$

Thirdly, $m \cdot d\boldsymbol{V}_K/dt = \Sigma F$ is still utilized, and the reference frame is the airflow axis system. We have

$$\begin{bmatrix} \dot{V}_A \\ 0 \\ 0 \end{bmatrix} + \begin{bmatrix} \dot{u}_{Wa} \\ \dot{v}_{Wa} \\ \dot{w}_{Wa} \end{bmatrix} + \begin{vmatrix} i & j & k \\ -\dot{\chi}_a \sin\gamma_a & \dot{\gamma}_a & \dot{\chi}_a \cos\gamma_a \\ \dot{V}_A & 0 & 0 \end{vmatrix}$$
$$= \frac{1}{m}\left\{\begin{bmatrix} -D \\ Y \\ -L \end{bmatrix} + T_{ab}\begin{bmatrix} T_{xb} \\ T_{yb} \\ T_{zb} \end{bmatrix} + T_{ag}\begin{bmatrix} 0 \\ 0 \\ mg \end{bmatrix}\right\}. \quad (7)$$

Rearranging this equation yields

$$\begin{bmatrix} \dot{V}_A \\ (V_A \cos\gamma_a)\cdot\dot{\chi}_a \\ -V_A \cdot \dot{\gamma}_a \end{bmatrix} = \frac{1}{m}\left\{\begin{bmatrix} -D \\ Y \\ -L \end{bmatrix} + T_{ab}\begin{bmatrix} T_{xb} \\ T_{yb} \\ T_{zb} \end{bmatrix} + T_{ag}\begin{bmatrix} 0 \\ 0 \\ mg \end{bmatrix}\right\} - T_{ag}\begin{bmatrix} \dot{u}_{Wg} \\ \dot{v}_{Wg} \\ \dot{w}_{Wg} \end{bmatrix}. \quad (8)$$

Then, in order to get the state equation of μ, we need the following relationship:

$$\dot{\mu} = \sin\gamma_a \cdot \dot{\chi}_a - \sin\beta \cdot \dot{\alpha} + p_K \cos\beta\cos\alpha + r_K \cos\beta\sin\alpha + q_K \sin\beta. \quad (9)$$

Substituting $\dot{\alpha}$ and $\dot{\chi}_a$ of (6) and (8) into (9), we can obtain $\dot{\mu}$. Now the state equations of x_g, y_g, z_g, V_A, χ_a , γ_a, α, β and μ have been gotten. Their last items denote the wind shear described by

$$\begin{bmatrix} \dot{u}_{Wg} \\ \dot{v}_{Wg} \\ \dot{w}_{Wg} \end{bmatrix} = \begin{bmatrix} u_{wx}\cdot\dot{x}_g + u_{wy}\cdot\dot{y}_g + u_{wz}\cdot\dot{z}_g \\ v_{wx}\cdot\dot{x}_g + v_{wy}\cdot\dot{y}_g + v_{wz}\cdot\dot{z}_g \\ w_{wx}\cdot\dot{x}_g + w_{wy}\cdot\dot{y}_g + w_{wz}\cdot\dot{z}_g \end{bmatrix}, \quad (10)$$

where wind field gradients $u_{wx} = \partial u_{Wg}/\partial x_g$, $v_{wy} = \partial v_{Wg}/\partial y_g$, $w_{wz} = \partial w_{Wg}/\partial z_g$, etc. Eq. (1) can be rewritten as

$$\begin{bmatrix} \dot{x}_g \\ \dot{y}_g \\ \dot{z}_g \end{bmatrix} = \begin{bmatrix} u_{Kg} \\ v_{Kg} \\ w_{Kg} \end{bmatrix} = T_{gk}\begin{bmatrix} V_K \\ 0 \\ 0 \end{bmatrix}, \quad (11)$$

where $[V_K, 0, 0]^{\mathrm{T}}$ is the expression of $\boldsymbol{V}_K$ in the path axis system and V_K is the module value of $\boldsymbol{V}_K$. Substituting (11) into (10) yields the derivative of wind vector.

Finally, using the angular motion equation of NHVs, i.e. $dH/dt = \sum M$ [14], we have

$$\begin{bmatrix} \dot{p}_K \\ \dot{q}_K \\ \dot{r}_K \end{bmatrix} = \begin{bmatrix} -(I_z - I_y)/I_x \cdot q_K \cdot r_K + l_A/I_x \\ -(I_x - I_z)/I_y \cdot p_K \cdot r_K + m_A/I_y \\ -(I_y - I_x)/I_z \cdot p_K \cdot q_K + n_A/I_z \end{bmatrix} + \begin{bmatrix} 1/I_x & 0 & 0 \\ 0 & 1/I_y & 0 \\ 0 & 0 & 1/I_z \end{bmatrix} \cdot M_C, \tag{12}$$

where H is the momentum moment and M is the total moment. I_x, I_y and I_z are moments of inertia. $M_C = g_{f,\delta}\delta_C$ represents the moment produced by all control surfaces. l_A, m_A and n_A are aerodynamic moments and they are functions of V_A, α, β, p_A, q_A, r_A, etc. p_A, q_A and r_A can be expressed as

$$\begin{bmatrix} p_A \\ q_A \\ r_A \end{bmatrix} = \begin{bmatrix} p_K \\ q_K \\ r_K \end{bmatrix} - \begin{bmatrix} p_W \\ q_W \\ r_W \end{bmatrix} = \begin{bmatrix} p_K \\ q_K \\ r_K \end{bmatrix} - \begin{bmatrix} w_{wy} \\ -w_{wx} \\ v_{wx} \end{bmatrix}, \tag{13}$$

where $[p_A, q_A, r_A]^{\mathrm{T}}$ is the NHV angular rate vector with respect to the airflow field and $[p_W, q_W, r_W]^{\mathrm{T}}$ is the angular rate of airflow field with respect to the ground. Besides, the wind gradients $w_{wy} = \partial w_{Wg}/\partial y_g$, $w_{wx} = \partial w_{Wg}/\partial x_g$ and $v_{wx} = \partial v_{Wg}/\partial x_g$. Because $[p_A, q_A, r_A]^{\mathrm{T}}$ cannot be measured and $[p_K, q_K, r_K]^{\mathrm{T}}$ is able to be obtained by rate gyro, we substitute (13) into (12) and get

$$\begin{bmatrix} \dot{p}_K \\ \dot{q}_K \\ \dot{r}_K \end{bmatrix} = \begin{bmatrix} -(I_z - I_y)/I_x \cdot q_K \cdot r_K + l_{A0}/I_x \\ -(I_x - I_z)/I_y \cdot p_K \cdot r_K + m_{A0}/I_y \\ -(I_y - I_x)/I_z \cdot p_K \cdot q_K + n_{A0}/I_z \end{bmatrix} + \begin{bmatrix} 1/I_x & 0 & 0 \\ 0 & 1/I_y & 0 \\ 0 & 0 & 1/I_z \end{bmatrix} \cdot M_C + \begin{bmatrix} \Delta l_A/I_x \\ \Delta m_A/I_y \\ \Delta n_A/I_z \end{bmatrix}, \tag{14}$$

where l_{A0}, m_{A0} and n_{A0} are in relation to $[p_K, q_K, r_K]^{\mathrm{T}}$, and Δl_A, Δm_A and Δn_A represent the items induced by wind gradients. $[p_K, q_K, r_K]^{\mathrm{T}}$ can also be written as $[p, q, r]^{\mathrm{T}}$.

Thus (2), (6), (8), (9) and (14) constitute 12 states equations with atmospheric disturbances. Their last items embody the wind impact. Since it is difficult to measure wind shear and turbulence in hypersonic flight, we need to design adaptive controllers to compensate for the effect of atmospheric disturbances.

3 Attitude controller design of the NHV

3.1 The NGPC law with disturbances

Owing to the strong nonlinearity and coupling of the NHV's model, nonlinear control methodologies become necessary means to its controller design. The nominal NGPC [9] is an effective NPC law designed in continuous-time domain. It can be applied to the NHV attitude controller design [7]. By (6), (9) and (14), the expressions of $\dot{\alpha}$, $\dot{\beta}$, $\dot{\mu}$, $\dot{p}_K$, $\dot{q}_K$ and $\dot{r}_K$ can be written as the affine nonlinear equations as

$$\begin{cases} \dot{\Omega} = f_s(\Omega) + g_s(\Omega) \cdot \omega_c + \Delta_s, \\ y_s = \Omega, \end{cases} \tag{15}$$

$$\begin{cases} \dot{\omega} = f_f(\omega) + g_f(\omega) \cdot M_C + \Delta_f, \\ y_f = \omega \end{cases} \tag{16}$$

where

$\Omega = [\alpha, \beta, \mu]^{\mathrm{T}}$ is the slow-loop state, the attitude angle vector. It is the output of the control system.

$\omega = [p, q, r]^{\mathrm{T}}$ is the fast-loop state which includes three angular velocities.

$M_C = g_{f,\delta}\delta_C \in \mathbb{R}^3$ is the control moment. $\delta_C = [\delta_e, \delta_a, \delta_r, \delta_x, \delta_y, \delta_z]^{\mathrm{T}}$ where δ_e, δ_a and δ_r denote the aero control surface deflection and δ_x, δ_y and δ_z represent the deflection of the thrust vector control surfaces. $g_{f,\delta} \in \mathbb{R}^{3\times 6}$ is the control allocation matrix.

$g_s \in \mathbb{R}^{3\times 3}$ and $g_f \in \mathbb{R}^{3\times 3}$ are invertible matrices, and $f_s, f_f \in \mathbb{R}^3$. The expressions of above matrices can be derived from (6), (9) and (14). In general, f_s, f_f, g_s and g_f are the nonlinear functions of Ω, ω, flight velocity, thrust, aerodynamic coefficients and aerodynamic moment coefficients.

$\Delta_s = [\Delta_\alpha, \Delta_\beta, \Delta_\mu]^{\mathrm{T}}$ and $\Delta_f = [\Delta_p, \Delta_q, \Delta_r]^{\mathrm{T}}$ are lumped disturbances upon the slow and fast loop respectively. They include parameter uncertainties, moment disturbances and atmospheric disturbances.

Systems (15) and (16) satisfy the assumptions [9]: The zero dynamics are stable, all states are available, the system input and lumped disturbances have the relative degree $\bar{\rho}$ [15] and Assumption 1.

Assumption 1. The unknown disturbances in systems (15) and (16) are bounded, i.e., $|\Delta_i| \leqslant \nu_i$, $i = 1, \ldots, 3$.

Remark 1. In practice, the exact bound value is not necessary, and any number larger than ν_i can be used.

The control purpose is to design a controller such that the closed-loop system is asymptotically stable and the output y optimally tracks a reference output y_r, in terms of a given performance index as

$$J = \frac{1}{2}\int_0^T e^{\mathrm{T}}(t+\tau)e(t+\tau)d\tau, \tag{17}$$

where T is the predictive period. e is the predictive tracking error, defined by $e(t+\tau) = y(t+\tau) - y_r(t+\tau)$ with $y(t+\tau)$ the predictive output during T and $y_r(t+\tau)$ the prescribed reference output.

For the NHV model, the state variable ω is the first to be affected, so the first step is to design fast-loop controller. In (16), ω is the fast-loop output. ω_r is the fast-loop reference output and it is actually the control vector ω_c in (15). Within the predictive period T_f, $\omega(t+\tau)$ and $\omega_r(t+\tau)$ at the time τ are approximately predicted by their Taylor-series expansions up to $(\bar{\rho}+\bar{r})$ th order. That is,

$$y_f(t+\tau) = \omega(t+\tau) \cong \Gamma(\tau)\bar{Y}(t), \quad y_{fr}(t+\tau) = \omega_r(t+\tau) \cong \Gamma(\tau)\bar{Y}_r(t), \tag{18}$$

where $\Gamma(\tau) = [I_3 \quad \bar{\tau} \quad \cdots \quad \bar{\tau}^{\bar{\rho}+\bar{r}}/(\bar{\rho}+\bar{r})!]$, $\bar{\tau} = \mathrm{diag}(\tau, \tau, \tau)$, $\bar{Y}(t) = [\omega(t)^{\mathrm{T}}, \dot{\omega}(t)^{\mathrm{T}}, \ldots, \omega^{[\bar{\rho}+\bar{r}]}(t)^{\mathrm{T}}]^{\mathrm{T}}$, $\bar{Y}_r(t) = [\omega_r(t)^{\mathrm{T}}, \dot{\omega}_r(t)^{\mathrm{T}}, \ldots, \omega_r^{[\bar{\rho}+\bar{r}]}(t)^{\mathrm{T}}]^{\mathrm{T}}$ and I_3 is a 3×3 unit matrix.

Repeated differentiating $\omega(t)$ in (16) up to $\bar{\rho}+\bar{r}$ times with respect to t, we obtain

$$\begin{aligned}
&\dot{\omega}(t) = f_f(\omega(t)) + g_f(\omega(t))M_c(t) + \Delta_f(\omega, M_c, t),\\
&\quad\vdots\\
&\omega^{[\bar{\rho}]}(t) = L_{f_f}^{\bar{\rho}}\omega(t) + L_{g_f}L_{f_f}^{\bar{\rho}-1}\omega(t)M_c(t) + L_{I_3}L_{f_f}^{\bar{\rho}-1}\omega(t)\Delta_f(\omega, M_c, t),\\
&\quad\vdots\\
&\omega^{[\bar{\rho}+\bar{r}]}(t) = L_{f_f}^{\bar{\rho}+\bar{r}}\omega(t) + p_{\bar{r}1}(M_c(t), \omega(t), \Delta_f) + \cdots +\\
&\qquad p_{\bar{r}\bar{r}}(M_c^{[\bar{r}-1]}(t), \ldots, M_c(t), \omega(t), \Delta_f) + L_{g_f}L_{f_f}^{\bar{\rho}-1}\omega(x)M_c^{[\bar{r}]}(t),
\end{aligned} \tag{19}$$

where $\bar{\rho}$ is the system relative degree and $\bar{\rho}$=1 for the NHV fast-loop system. $p_{11}, \ldots, p_{\bar{r}1}, \ldots, p_{\bar{r}\bar{r}}$ are the complicated functions in terms of M_c, $\dot{M}_c$, $M_c^{[\bar{r}-1]}$ and ω. The standard Lie notation is used here. $\bar{r}$ is the control order [9] which is often set zero for the realization simplicity.

Then from (18), the index (17) becomes

$$J = \frac{1}{2}(\bar{Y}(t) - \bar{Y}_r(t))^{\mathrm{T}} \cdot \int_0^{T_f} \Gamma^{\mathrm{T}}(\tau)\Gamma(\tau)d\tau \cdot (\bar{Y}(t) - \bar{Y}_r(t)). \tag{20}$$

Substituting (19) into (20) and letting $\partial J/\partial M_c|_{M_c=M_c^*} = 0$, we can derive the fast-loop control law as

$$M_C(t) = u_f = -g_f^{-1}(f_f + K_f e_f - \dot{\omega}_r) - g_f^{-1}\Delta_f = \bar{M} - g_f^{-1}\Delta_f, \tag{21}$$

where $\bar{M} = -g_f^{-1}(f_f + K_f e_f - \dot{\omega}_r)$ denotes the nominal control law. The fast-loop error e_f equals $\omega - \omega_r$ and K_f is composed of the first 3 rows of $\bar{\Gamma}_{\bar{r}\bar{r}}^{-1} \cdot \bar{\Gamma}_{\bar{\rho}\bar{r}}^{\mathrm{T}}$. Depending on its definition in [9], we have

$$\begin{aligned}
K_f &= \bar{\Gamma}_{(2,2)}^{-1} \cdot \bar{\Gamma}_{(1,2)}^{\mathrm{T}}\\
&= \mathrm{diag}\{3/T_f^3, 3/T_f^3, 3/T_f^3\} \cdot \mathrm{diag}\{T_f^2/2, T_f^2/2, T_f^2/2\}
\end{aligned}$$

$$= \mathrm{diag}\{3/(2T_f), 3/(2T_f), 3/(2T_f)\}. \tag{22}$$

The control law of the slow-loop is similarly given by

$$\omega_c(t) = u_s = -g_s^{-1}(f_s + K_s e_s - \dot{\Omega}_r) - g_s^{-1}\Delta_s = \bar{\omega} - g_s^{-1}\Delta_s, \tag{23}$$

where $e_s = \Omega - \Omega_r$, $K_s = \mathrm{diag}\{3/(2T_s), 3/(2T_s), 3/(2T_s)\}$ and T_s is the slow-loop predictive time.

Since ω_c is the reference value of the fast-loop system, replacing ω_r in (21) with ω_c in (23) will yield the control moment M_c of the whole attitude system. Then, the control vector δ_C is equal to $g_{f,\delta}^{-1} \cdot M_C$.

Remark 2. There are only K_f and K_s which need to be designed in the nominal control law $\bar{M}$ and $\bar{\omega}$. The matrices K_f and K_s depend on the predictive time T_f and T_s given in advance. Therefore, the nominal NGPC is a quite efficient algorithm for the realization of the NHV controller.

3.2 The BRFLN-based adaptive NGPC

Since Δ_f and Δ_s in (21) and (23) are practically unknown, it is very necessary to replace them by $\hat{\Delta}_f$ and $\hat{\Delta}_s$ which can be calculated. Suppose that v_{adf} is the estimation of $\hat{\Delta}_f$, and let v_{rf} denote the estimation error (i.e. $v_{rf} = \hat{\Delta}_f - v_{adf}$). Then the fast-loop control law can be designed as

$$M_C = \bar{M} - g_f^{-1}\hat{\Delta}_f = \bar{M} - M_{ad} - M_r,\ M_{ad} = g_f^{-1} \cdot v_{adf},\ M_r = g_f^{-1} \cdot v_{rf}, \tag{24}$$

where M_{ad} is the control adjustment. M_r denotes a robust control (RC) item used for offsetting the error between $\hat{\Delta}_f$ and v_{adf}. The control law of the slow-loop is similar to that of the fast-loop. It is

$$\omega_c = \bar{\omega} - g_s^{-1}\hat{\Delta}_s = \bar{\omega} - \omega_{ad} - \omega_r,\ \omega_{ad} = g_s^{-1} \cdot v_{ads},\ \omega_r = g_s^{-1} \cdot v_{rs}, \tag{25}$$

where v_{ads} is the estimation of $\hat{\Delta}_s$ and $v_{rs} = \hat{\Delta}_s - v_{ads}$.

Δ_f and Δ_s are dynamically changeable functions, so dynamic mapping methods generally are fit for their approximation better than static ones. Consequently, a new RNN-based method, the BRFLN adaptive NGPC is proposed to estimate the lumped disturbances. Figure 2 shows the structure of the presented method. In this figure, W_f and W_s are the fast-loop weight matrix and the slow-loop weight matrix, respectively. They are both in need of online learning. Additionally, the RC gains, i.e. ψ_f and ψ_s, have their adaptive laws which can lead to less conservative controller design and weaken the chattering of the control vectors.

Because the dynamic property of the fast-loop system differs from that of the slow-loop system, there are some differences between the controller designs of the two loops. As Figure 2 shows, the control effect of the slow-loop BRFLN and RC must pass through the fast dynamics of the NHV, and then it can influence the slow dynamics of the NHV, whereas the effect of the slow-loop disturbances Δ_s on the NHV's slow dynamics is just instantaneous. That is, there exists time difference between the two kinds of effect. Hence, we propose a solution that the proportional-derivative (PD) lead compensation is introduced in the slow-loop BRFLN and RC design so as to offset the time difference. As a result, the PD correction BRFLN and RC in the slow-loop controller may counteract the harmful effect that Δ_s produces. The BRFLN design will be presented in the next section.

3.3 The design of BRFLN

FLN is a single-layer NN and it is capable of forming arbitrarily complex decision regions [10]. The prime advantage of the FLN is its reduced computational complexity without any sacrifice on its performance [10–12]. In order to approximate dynamical uncertainties during hypersonic flight, we propose a new RNN, the BRFLN. Since a feedforward network combined with recurrent feedback and input time delays can effectively capture the optimal temporal profiles of a dynamical system [16], the FLN outputs are directly fed into the input layer to build the structure of BRFLN. In addition, we add the self-feedback links on the context nodes so as to simulate high-order systems, which is one of the differences between the PFFLN [7] and the BRFLN. The BRFLN does not have hidden layers, which greatly reduces the computing loads of the network and enables the BRFLN to be employed in the online training. The architecture can be shown as Figure 3.

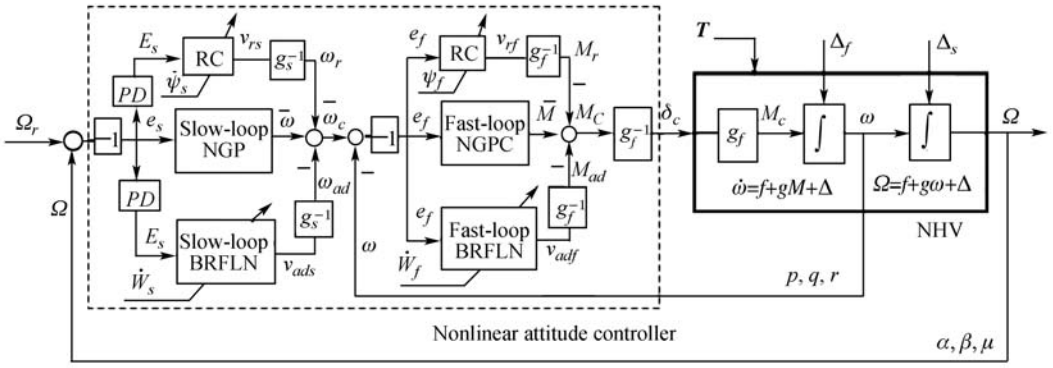

Figure 2 The BRFLN-based NGPC design of the NHV.

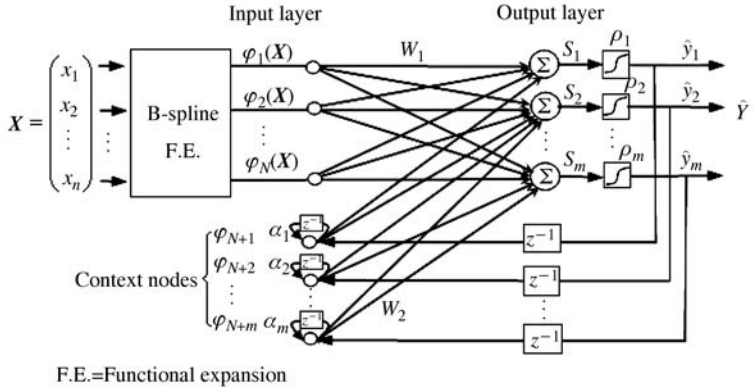

Figure 3 Structure of the BRFLN.

Suppose that the function set $\mathcal{B} = \{\varphi_k \in \Phi(A)\}_{k\in K}(K = 1, \ldots, N)$ satisfies: 1) $\varphi_1 = 1$; 2) the subset $\mathcal{B}_j = \{\varphi_i \in \mathcal{L}(A)\}_{i=1}^{j}$ is a linearly independent set; 3) $\sup_j[\sum_{i=1}^{j} \|\varphi_i\|_A^2]^{1/2} < \infty$. Hence, we can expand the input $X \in A \subset \mathbb{R}^n$ into the functionally mapped inputs by $\mathcal{B}$. Then $\hat{Y}$ can be expressed as

$$v_{ad} = \hat{Y}(k+1) = \rho(W^{\mathrm{T}}\Phi(X(k+1), \hat{Y}(k), \hat{\alpha}(k))), \tag{26}$$

where $W = [W_1{}^{\mathrm{T}}, W_2{}^{T}]^{\mathrm{T}}$ is the weight matrix. $W_1 \in \mathbb{R}^{m\times N}$ is the feedforward weight matrix and $W_2 \in \mathbb{R}^{m\times m}$ is the feedback one. Besides, $\Phi = [\Phi_1{}^{\mathrm{T}}(X), \Phi_2{}^{\mathrm{T}}(\hat{Y}, \hat{\alpha})]^{\mathrm{T}} \in \mathbb{R}^{N+m}$. $\Phi_1(X) = [\varphi_1(X), \varphi_2(X), \ldots, \varphi_N(X)]^{\mathrm{T}} \in \mathbb{R}^N$ is the basis function matrix and $\hat{\alpha} = [\alpha_1, \ldots, \alpha_m]^{\mathrm{T}}$ is the self-connection weight matrix.

As mentioned previously, the basis functions (i.e. $\mathcal{B}$) are orthogonal functions. They typically include Chebyshev, Legendre, Lagrange, Hermite polynomials, etc. Different from the traditional FLN and the PFFLN, the proposed network employs B-spline basis functions for the first time. In many application fields, the spline curve approximation is attractive in terms of some properties such as continuity, local controllability, low approximation error and simple implementation. It can reach a higher accuracy than polynomials approximation. So in this research, we utilize the central B-spline basis functions as the input expansion functions. The n-degree B-spline functions [17] are recursively defined by

$$N_1(x) = \begin{cases} -|x| + 1, & |x| < 1, \\ 0, & |x| \geqslant 1, \end{cases}$$

$$N_2(x) = \begin{cases} -x^2 + 3/4, & |x| \leqslant 1/2, \\ 1/2 \cdot (x^2 - 3|x| + 9/4), & 1/2 \leqslant |x| \leqslant 3/2, \end{cases}$$

$$N_3(x) = \begin{cases} 1/2 \cdot |x|^3 - x^2 + 2/3, & |x| \leqslant 1, \\ -1/6 \cdot |x|^3 + x^2 - 2|x| + 4/3, & 1 < |x| < 2, \ldots, \end{cases}$$

$$N_n(x) = \sum_{j=0}^{n+1}(-1)^j C_{n+1}^j \cdot \left(x + \frac{n+1}{2} - j\right)_+^n / n!, \quad -\infty < x < \infty, \tag{27}$$

where $C_{n+1}^j = \frac{(n+1)!}{j!(n+1-j)!}$ is the combination formula and $(x+a)_+^n = \begin{cases} (x+a)^n & x+a \geqslant 0 \\ 0 & x+a<0 \end{cases}$. The support set of B-spline functions, the x value range can be described by $SuppN_n \subseteq (-(n+1)/2, (n+1)/2)$. And $N_i = 0$ when x is outside of $SuppN_i$. Generally, we are concerned with cubic B-spline functions (order $n \leqslant 3$) because they are simple for implementation and most frequently used in practice. That is,

$$\Phi_1(X) = [1, N_1(x_1), N_2(x_1), N_3(x_1), N_1(x_2), N_2(x_2), N_3(x_2), \ldots, N_1(x_n), N_2(x_n), N_3(x_n)]^{\mathrm{T}} \in \mathbb{R}^N.$$

And the input X must be normalized within the set which is $U = (SuppN_1 \cap SuppN_2 \cap SuppN_3) \subseteq (-1, 1)$.

It is noted that the input layer consists of the F.E. outputs and the context nodes outputs. The latter is denoted by $\Phi_2(\hat{Y}, \hat{\alpha}) = [\varphi_{N+1}, \varphi_{N+2}, \ldots, \varphi_{N+m}]^{\mathrm{T}} \in \mathbb{R}^m$, and φ_i satisfies

$$\varphi_\iota(t+1) = \alpha_p \varphi_\iota(t) + \hat{y}_p(t) \qquad |\varphi_\iota| \leqslant 1, \quad i = N+1, \ldots, N+m; \quad p = 1, \ldots, m, \tag{28}$$

where $\varphi_i(t+1)$ represents the node output at the instant $t+1$, and α_p $(0 \leqslant \alpha_p < 1)$ is the self-connection weight. If the recursion operation is performed for $\varphi_i(t+1)$, we have

$$\varphi_\iota(t) = \alpha_p \varphi_\iota(t-1) + \hat{y}_p(t-1), \ldots, \varphi_\iota(t-n) = \alpha_p \varphi_\iota(t-n-1) + \hat{y}_p(t-n-1), \ldots$$

Then (28) can be written as

$$\varphi_\iota(t+1) = \hat{y}_p(t) + \alpha_p \hat{y}_p(t-1) + \alpha_p^2 \hat{y}_p(t-2) + \cdots + \alpha_p^n \hat{y}_p(t-n) + \cdots = \sum_{\tau=0}^{t} \alpha_p^\tau \hat{y}_p(t-\tau). \tag{29}$$

Expression (29) indicates that the closer α_p gets to 1, the further moment of $\hat{y}_p$ will be considered. Hence the self-connection endues the nodes with capacity to memorize a certain past of their input data and simulate high-order dynamical systems. The weight α_p can be obtained by training, but an easier way to do it is to fix it a priori. In addition, $\rho(S) = (\rho_1, \rho_2, \ldots, \rho_m)^{\mathrm{T}}$ is defined by

$$\rho_j = \tanh(S_j) = (1 - \mathrm{e}^{-2S_j})/(1 + \mathrm{e}^{-2S_j}), \quad \rho_j' = 1 - \rho_j^2, \quad j = 1, 2, \ldots, m, \tag{30}$$

where $S = W^{\mathrm{T}}\Phi = [S_1, S_2, \ldots, S_m]^{\mathrm{T}}$.

If the BRFLN is employed for approximating disturbances, we need to provide Definition 1.

Definition 1. On the compact region $D_e \subset \mathbb{R}^m$, define the optimal weights and output of the BRFLN as

$$W^* = \arg\min_W \left\{ \sup_{e \in D_e} \|\Delta - v_{ad}\| \right\}, \tag{31}$$

$$v_{ad}^* = \rho({W^*}^{\mathrm{T}} \Phi(X, \hat{Y}, \hat{\alpha})) = \Delta - \varepsilon, \quad \|\varepsilon\| \leqslant \psi_\varepsilon^*, \tag{32}$$

where e is the input vector of the BRFLN, W^* satisfies $\|W^*\| \leqslant \bar{W}$ and $\|\cdot\|$ denotes the Frobenius norm. ε is the approximation error and $\psi_\varepsilon^* \geqslant 0$ is an unknown bound.

4 The stability analysis of close-loop system

It is necessary to obtain the error state equation of the closed-loop system before the stability analysis. From (16) and (24), the fast-loop error state equation is expressed as

$$\dot{e}_f = \dot{\omega} - \dot{\omega}_r = f_f + g_f(\bar{M} - g_f^{-1}\hat{\Delta}_f) + \Delta_f - \dot{\omega}_r = -K_f e_f + (\Delta_f - \hat{\Delta}_f) = A_f e_f + (\Delta_f - \hat{\Delta}_f). \tag{33}$$

Utilizing (31), (32) and the Taylor series expansion for $\rho({W^*}^{\mathrm{T}}\Phi)$, we have

$$\Delta_f - \hat{\Delta}_f = \rho(W_f^{*\mathrm{T}} \Phi_f) + \varepsilon_f - \rho(W_f^{\mathrm{T}} \Phi_f) - v_{rf}$$

$$= \rho(W_f^{\mathrm{T}}\Phi_f) + \rho'_f\tilde{W}_f^{\mathrm{T}}\Phi_f + o(\tilde{W}_f^{\mathrm{T}}\Phi_f)^2 + \varepsilon_f - \rho(W_f^{\mathrm{T}}\Phi_f) - v_{rf}$$
$$= \rho'_f\tilde{W}_f^{\mathrm{T}}\Phi_f + o(\tilde{W}_f^{\mathrm{T}}\Phi_f)^2 + \varepsilon_f - v_{rf}, \tag{34}$$

where the weight error $\tilde{W}_f = W_f^* - W_f$, $\rho'_f = \rho'(W_f^{\mathrm{T}}\Phi_f) = d\rho/d\nu|_{\nu=W_f^{\mathrm{T}}\Phi_f}$ and $o(\tilde{W}_f^{\mathrm{T}}\Phi_f)^2$ represents higher-order terms. Substituting (34) into (33), we have the fast-loop error state equation described by

$$\dot{e}_f = A_f e_f + \rho'_f\tilde{W}_f^{\mathrm{T}}\Phi_f + o(\tilde{W}_f^{\mathrm{T}}\Phi_f)^2 + \varepsilon_f - v_{rf}. \tag{35}$$

Now using Taylor expansion for $\rho(W^{*\mathrm{T}}\Phi)$, we have

$$z_f^{\mathrm{T}}o(\tilde{W}_f^{\mathrm{T}}\Phi_f)^2 = z_f^{\mathrm{T}}\rho(W_f^{*\mathrm{T}}\Phi_f) - z_f^{\mathrm{T}}\rho(W_f^{\mathrm{T}}\Phi_f) - z_f^{\mathrm{T}}\rho'_f W_f^{*\mathrm{T}}\Phi_f + z_f^{\mathrm{T}}\rho'_f W_f^{\mathrm{T}}\Phi_f,$$

where $z_f \in \mathbb{R}^3$ will be mentioned in Theorem 1. So,

$$|z_f^{\mathrm{T}}o(\tilde{W}_f^{\mathrm{T}}\Phi_f)^2| \leqslant |\rho(W_f^{*\mathrm{T}}\Phi_f) - \rho(W_f^{\mathrm{T}}\Phi_f)|\|z_f\|_1 + \mathrm{tr}(\rho'_f W_f^{\mathrm{T}}\Phi_f z_f^{\mathrm{T}}) - \mathrm{tr}(W_f^{*\mathrm{T}}\Phi_f z_f^{\mathrm{T}}\rho'_f)$$
$$\leqslant \psi_{wf}^*\sigma_{wf}\|z_f\|, \tag{36}$$

where $\|\cdot\|_1$ is the absolute value sum of matrix elements, $\sigma_{wf} = (\|z_f\|_1 + \|\rho'_f W_f^{\mathrm{T}}\Phi_f z_f^{\mathrm{T}}\| + \|\Phi_f z_f^{\mathrm{T}}\rho'_f\|)/\|z_f\|$ and $\psi_{wf}^* = \max\{2, 1, \|W_f^*\|\}$. In addition, we define

$$\psi_{mf}^* = \max\{\psi_{wf}^*, \psi_{\varepsilon f}^*\}, \quad \tilde{\psi}_f = \psi_{mf}^* - \psi_f, \tag{37}$$

where the definition of $\psi_{\varepsilon f}^*$ is the same as that of ψ_ε^* in (32), and $\tilde{\psi}_f$ is the estimation error of robust gain.

Similarly, the application of (15) and (25) yields the slow-loop error state equation as

$$\dot{e}_s = \dot{\Omega} - \dot{\Omega}_r = A_s e_s + (\Delta_s - \hat{\Delta}_s). \tag{38}$$

As illustrated in Figure 2, we employ E_s as the input of the slow-loop BRFLN and RC. E_s and e_s satisfy

$$E_s = K_p e_s + K_d \dot{e}_s, \tag{39}$$

where K_p is the proportional coefficient, and K_d is the derivative coefficient.

Substituting (38) into (39), we get

$$\dot{E}_s = K_p\dot{e}_s + K_d\ddot{e}_s = K_p(A_s e_s + \Delta_s - \hat{\Delta}_s) + K_d(A_s\dot{e}_s + \dot{\Delta}_s - \dot{\hat{\Delta}}_s)$$
$$= A_s E_s + (K_p\Delta_s + K_d\dot{\Delta}_s) - (K_p\hat{\Delta}_s + K_d\dot{\hat{\Delta}}_s). \tag{40}$$

Because $K_p\Delta_s + K_d\dot{\Delta}_s$ is the expression of proportional-derivative (PD) lead compensation, $\dot{E}_s$ is approximately expressed as

$$\dot{E}_s = A_s E_s + \bar{\Delta}_s(t - \tau_0) - \hat{\bar{\Delta}}_s(t - \tau_0), \tag{41}$$

where τ_0 is the lead time. Then, similar to (34), $\bar{\Delta}_s(t - \tau_0) - \hat{\bar{\Delta}}_s(t - \tau_0)$ is described by

$$\bar{\Delta}_s(t - \tau_0) - \hat{\bar{\Delta}}_s(t - \tau_0) = \rho'_s\tilde{W}_s^{\mathrm{T}}\Phi_s(E_s) + o(\tilde{W}_s^{\mathrm{T}}\Phi_s(E_s))^2 + \varepsilon_s - v_{rs}(E_s), \tag{42}$$

where the weight error $\tilde{W}_s = W_s^* - W_s$, $\rho'_s \triangleq \rho'(W_s^{\mathrm{T}}\Phi_s(E_s)) = d\rho/d\nu|_{\nu=W_s^{\mathrm{T}}\Phi_s(E_s)}$. Moreover,

$$|z_s^{\mathrm{T}}o(\tilde{W}_s^{\mathrm{T}}\Phi_s(E_s))^2| \leqslant \psi_{ws}^*\sigma_{ws}\|z_s\|, \tag{43}$$

where $\sigma_{ws} = (\|z_s\|_1 + \|\rho'_s W_s^{\mathrm{T}}\Phi_s(E_s)z_s^{\mathrm{T}}\| + \|\Phi_s(E_s)z_s^{\mathrm{T}}\rho'_s\|)/\|z_s\|$ and $\psi_{ws}^* = \max\{2, 1, \|W_s^*\|\}$. In addition, we define

$$\psi_{ms}^* = \max\{\psi_{ws}^*, \psi_{\varepsilon s}^*\}, \quad \tilde{\psi}_s = \psi_{ms}^* - \psi_s, \tag{44}$$

where the definition of $\psi_{\varepsilon s}^*$ comes from (32), and $\tilde{\psi}_s$ is the estimation error of the slow-loop robust gain.

Now the closed-loop stability analysis of the proposed control scheme can be presented by Theorem 1.

Theorem 1. Assume that systems (16) and (15) are controlled by (24), (25), (45) and (47). If the online adjustment parameters are tuned by (46) and (48), then the system errors (e_f, E_s) and the estimation errors ($\tilde{W}_f$,$\tilde{\psi}_f$, $\tilde{W}_s$,$\tilde{\psi}_s$) are uniformly ultimately bounded.

$$v_{adf} = \rho(W_f^{\mathrm{T}}\Phi_f), \quad v_{rf} = \psi_f\sigma_f^* \tanh(\sigma_f^* z_f/\delta_f), \quad z_f = P_f e_f(t), \tag{45}$$

$$\dot{W}_f = \Gamma_{Wf}(\Phi_f z_f^{\mathrm{T}}\rho_f' - K_{Wf}W_f), \dot{\psi}_f = \lambda_{\psi f}(\sigma_f^* z_f^{\mathrm{T}} \tanh(\sigma_f^* z_f/\delta_f) - K_{\psi f}\psi_f), \tag{46}$$

$$v_{ads} = \rho(W_s^{\mathrm{T}}\Phi_s), \quad v_{rs} = \psi_s\sigma_s^* \tanh(\sigma_s^* z_s/\delta_s), \quad z_s = P_s E_s(t), \tag{47}$$

$$\dot{W}_s = \Gamma_{Ws}(\Phi_s(E_s) z_s^{\mathrm{T}}\rho_s' - K_{Ws}W_s), \quad \dot{\psi}_s = \lambda_{\psi s}(\sigma_s^* z_s^{\mathrm{T}} \tanh(\sigma_s^* z_s/\delta_s) - K_{\psi s}\psi_s), \tag{48}$$

where $\sigma_f^* = \sigma_{wf} + 1$ and $\sigma_s^* = \sigma_{ws} + 1$. δ_f, K_{Wf}, $\lambda_{\psi f}$, $K_{\psi f}$, δ_s, K_{Ws}, $\lambda_{\psi s}$ and $K_{\psi s}$ are positive design constants. Γ_{Wf} and Γ_{Ws} are positive definite matrices. $\tanh(x)$ denotes the hyperbolic tangent function.

Proof. Let the Lyapunov function candidate be given by

$$V = \frac{1}{2}e_f^{\mathrm{T}}P_f e_f + \frac{1}{2}\mathrm{tr}(\tilde{W}_f^{\mathrm{T}}\Gamma_{Wf}^{-1}\tilde{W}_f) + \frac{1}{2\lambda_{\psi f}}\tilde{\psi}_f^2 + \frac{1}{2}E_s^{\mathrm{T}}P_s E_s + \frac{1}{2}\mathrm{tr}(\tilde{W}_s^{\mathrm{T}}\Gamma_{Ws}^{-1}\tilde{W}_s) + \frac{1}{2\lambda_{\psi s}}\tilde{\psi}_s^2, \tag{49}$$

where P_f and P_s are positive definite matrices satisfying

$$\begin{aligned} &P_f A_f + A_f^{\mathrm{T}}P_f = -Q_f, \quad P_f = P_f^{\mathrm{T}}, \quad Q_f = Q_f^{\mathrm{T}} > 0, \\ &P_s A_s + A_s^{\mathrm{T}}P_s = -Q_s, \quad P_s = P_s^{\mathrm{T}}, \quad Q_s = Q_s^{\mathrm{T}} > 0, \end{aligned} \tag{50}$$

where $A_f = -K_f$ and $A_s = -K_s$ are the coefficient matrices of (35) and (41).

Differentiating (49) and substituting (35), (37), (41), (42), (44) and (50) into $\dot{V}$ yields

$$\begin{aligned} \dot{V} = &\frac{1}{2}e_f^{\mathrm{T}}(A_f^{\mathrm{T}}P_f + P_f A_f)e_f + e_f^{\mathrm{T}}P_f[\Delta_f(t) - \hat{\Delta}_f(t)] + \mathrm{tr}(\tilde{W}_f^{\mathrm{T}}\Gamma_{Wf}^{-1}\dot{\tilde{W}}_f) + \frac{1}{\lambda_{\psi f}}\tilde{\psi}_f\dot{\tilde{\psi}}_f \\ &+ \frac{1}{2}E_s^{\mathrm{T}}(A_s^{\mathrm{T}}P_s + P_s A_s)E_s + E_s^{\mathrm{T}}P_s[\bar{\Delta}_f(t-\tau_0) - \hat{\bar{\Delta}}_f(t-\tau_0)] + \mathrm{tr}(\tilde{W}_s^{\mathrm{T}}\Gamma_{Ws}^{-1}\dot{\tilde{W}}_s) + \frac{1}{\lambda_{\psi s}}\tilde{\psi}_s\dot{\tilde{\psi}}_s \\ = &-\frac{1}{2}e_f^{\mathrm{T}}Q_f e_f + z_f^{\mathrm{T}}[\rho_f'\tilde{W}_f^{\mathrm{T}}\Phi_f + o(\tilde{W}_f^{\mathrm{T}}\Phi_f)^2 + \varepsilon_f - v_{rf}] - \mathrm{tr}(\tilde{W}_f^{\mathrm{T}}\Gamma_{Wf}^{-1}\dot{W}_f) - \frac{1}{\lambda_{\psi f}}\tilde{\psi}_f\dot{\psi}_f \\ &- \frac{1}{2}E_s^{\mathrm{T}}Q_s E_s + z_s^{\mathrm{T}}[\rho_s'\tilde{W}_s^{\mathrm{T}}\Phi_s(E_s) + o(\tilde{W}_s^{\mathrm{T}}\Phi_s(E_s))^2 + \varepsilon_s - v_{rs}(E_s)] - \mathrm{tr}(\tilde{W}_s^{\mathrm{T}}\Gamma_{Ws}^{-1}\dot{W}_s) - \frac{1}{\lambda_{\psi s}}\tilde{\psi}_s\dot{\psi}_s. \end{aligned}$$

Choosing the online tuning laws as (46) and (48), we get

$$\begin{aligned} \dot{V} = &-\frac{1}{2}e_f^{\mathrm{T}}Q_f e_f + z_f^{\mathrm{T}}o(\tilde{W}_f^{\mathrm{T}}\Phi_f)^2 + K_{Wf}\mathrm{tr}[\tilde{W}_f^{\mathrm{T}}(W_f^* - \tilde{W}_f)] + z_f^{\mathrm{T}}\varepsilon_f - \psi_f\sigma_f^* z_f^{\mathrm{T}} \tanh(\sigma_f^* z_f/\delta_f) \\ &+ \kappa_{\psi f}\tilde{\psi}_f\psi_f - \tilde{\psi}_f\sigma_f^* z_f^{\mathrm{T}} \tanh(\sigma_f^* z_f/\delta_f) - \frac{1}{2}E_s^{\mathrm{T}}Q_s E_s + z_s^{\mathrm{T}}o(\tilde{W}_s^{\mathrm{T}}\Phi_s(E_s))^2 + K_{Ws}\mathrm{tr}[\tilde{W}_s^{\mathrm{T}}(W_s^* - \tilde{W}_s)] \\ &+ z_s^{\mathrm{T}}\varepsilon_s + \kappa_{\psi s}\tilde{\psi}_s\psi_s - \psi_s\sigma_s^* z_s^{\mathrm{T}} \tanh(\sigma_s^* z_s/\delta_s) - \tilde{\psi}_s\sigma_s^* z_s^{\mathrm{T}} \tanh(\sigma_s^* z_s/\delta_s). \end{aligned}$$

Application of (32), (36), (37), (43) and (44) yields

$$\begin{aligned} \dot{V} \leqslant &-\frac{1}{2}\underline{\lambda}(Q_f)\|e_f\|^2 + \psi_{wf}^*\sigma_{wf}\|z_f\| + K_{Wf}\mathrm{tr}(\|\tilde{W}_f\|\bar{W}_f - \|\tilde{W}_f\|^2) - \psi_{mf}^*\sigma_f^* z_f^{\mathrm{T}} \tanh(z_f\sigma_f^*/\delta_f) \\ &+ \psi_{\varepsilon f}^*\|z_f\| + K_{\psi f}\tilde{\psi}(\psi_{mf}^* - \tilde{\psi}_f) - \frac{1}{2}\underline{\lambda}(Q_s)\|E_s\|^2 + \psi_{ws}^*\varsigma_{ws}\|z_s\| + K_{Ws}\mathrm{tr}(\|\tilde{W}_s\|\bar{W}_s - \|\tilde{W}_s\|^2) \\ &- \psi_{ms}^*\sigma_s^* z_s^{\mathrm{T}} \tanh(z_s\sigma_s^*/\delta_s) + \psi_{\varepsilon s}^*\|z_s\| + K_{\psi s}\tilde{\psi}_s(\psi_{ms}^* - \tilde{\psi}_s) \\ \leqslant &-\frac{1}{2}\underline{\lambda}(Q_f)\|e_f\|^2 + \sigma_f^*\psi_{mf}^*\|z_f\| - \psi_{mf}^*\sigma_f^* z_f^{\mathrm{T}} \tanh(z_f\sigma_f^*/\delta_f) + K_{Wf}(\|\tilde{W}_f\|\bar{W}_f - \|\tilde{W}_f\|^2) \\ &+ K_{\psi f}\left(\frac{1}{2}\psi_{mf}^{*2} - \frac{1}{2}\tilde{\psi}_f^2\right) - \frac{1}{2}\underline{\lambda}(Q_s)\|E_s|^2 + \sigma_s^*\psi_{ms}^*\|z_s\| - \psi_{ms}^*\sigma_s^* z_s^{\mathrm{T}} \tanh(z_s\sigma_s^*/\delta_s) \\ &+ K_{Ws}(\|\tilde{W}_s\|\bar{W}_s - \|\tilde{W}_s\|^2) + K_{\psi s}\left(\frac{1}{2}\psi_{ms}^{*2} - \frac{1}{2}\tilde{\psi}_s^2\right), \end{aligned} \tag{51}$$

where $\underline{\lambda}(\cdot)$ denotes the matrix minimum eigenvalue. Employing Lemma 1 in [18] results in

$$\sigma_f^*\psi_{mf}^*\|z_f\| - \psi_{mf}^*\sigma_f^* z_f^{\mathrm{T}}\tanh(z_f\sigma_f^*/\delta_f) \leqslant \psi_{mf}^*\xi\delta_f$$

and

$$\sigma_s^*\psi_{ms}^*\|z_s\| - \psi_{ms}^*\sigma_s^* z_s^{\mathrm{T}}\tanh(z_s\sigma_s^*/\delta_s) \leqslant \psi_{ms}^*\xi\delta_s,$$

where $\xi = 3 \times 0.2785$. Therefore, (51) becomes

$$\begin{aligned}\dot{V} \leqslant\ & -\frac{1}{2}\underline{\lambda}(Q_f)\|e_f\|^2 + \psi_{mf}^*\xi\delta_f + K_{Wf}\left(\frac{1}{2}\bar{W}_f^2 - \frac{1}{2}\|\tilde{W}_f\|^2\right) + \frac{1}{2}K_{\psi f}\psi_{mf}^{*2} - \frac{1}{2}K_{\psi f}\tilde{\psi}_f^2\\ & -\frac{1}{2}\underline{\lambda}(Q_s)\|E_s\|^2 + \psi_{ms}^*\xi\delta_s + K_{Ws}\left(\frac{1}{2}\bar{W}_s^2 - \frac{1}{2}\|\tilde{W}_s\|^2\right) + \frac{1}{2}K_{\psi s}\psi_{ms}^{*2} - \frac{1}{2}K_{\psi s}\tilde{\psi}_s^2. \end{aligned} \tag{52}$$

Define $C_f = 2\psi_{mf}^*\xi\delta_f + K_{Wf}\bar{W}_f^2 + K_{\psi f}\psi_{mf}^{*2} > 0$ and $C_s = 2\psi_{ms}^*\xi\delta_s + K_{Ws}\bar{W}_s^2 + K_{\psi s}\psi_{ms}^{*2} > 0$. Then (52) satisfies

$$\begin{aligned}\dot{V} \leqslant\ & -\frac{1}{2}\underline{\lambda}(Q_f)\|e_f\|^2 - \frac{1}{2}K_{Wf}\|\tilde{W}_f\|^2 - \frac{1}{2}K_{\psi f}\tilde{\psi}_f^2 + \frac{1}{2}C_f - \frac{1}{2}\underline{\lambda}(Q_s)\|E_s\|^2\\ & -\frac{1}{2}K_{Ws}\|\tilde{W}_s\|^2 - \frac{1}{2}K_{\psi s}\tilde{\psi}_s^2 + \frac{1}{2}C_s. \end{aligned} \tag{53}$$

Thus, $\dot{V}$ is negative when one of the following inequalities is satisfied,

$$\begin{aligned}&\|e_f\| > \sqrt{C_f/\underline{\lambda}(Q_f)} \text{ and } \|E_s\| > \sqrt{C_s/\underline{\lambda}(Q_s)},\\ &\|\tilde{W}_f\| > \sqrt{C_f/K_{Wf}} \text{ and } \|\tilde{W}_s\| > \sqrt{C_s/K_{Ws}},\\ &|\tilde{\psi}_f| > \sqrt{C_f/K_{\psi f}} \text{ and } |\tilde{\psi}_s| > \sqrt{C_s/K_{\psi s}}. \end{aligned} \tag{54}$$

Set $c_1 = \min(\underline{\lambda}(Q_f)/\bar{\lambda}(P_f), K_{Wf}\underline{\lambda}(\Gamma_{wf}), K_{\psi f}\lambda_{\psi f}, \underline{\lambda}(Q_s)/\bar{\lambda}(P_s), K_{Ws}\underline{\lambda}(\Gamma_{ws}), K_{\psi s}\lambda_{\psi s})$ and $c_2 = (C_s + C_f)/2$. Then (53) can be rewritten as

$$\begin{aligned}\dot{V} \leqslant\ & -\underline{\lambda}(Q_f)/\bar{\lambda}(P_f)\cdot\frac{1}{2}e_f^{\mathrm{T}}P_f e_f - K_{Wf}\underline{\lambda}(\Gamma_{wf})\cdot\frac{1}{2}\mathrm{tr}(\tilde{W}_f^{\mathrm{T}}\Gamma_{wf}^{-1}\tilde{W}_f) - K_{\psi f}\lambda_{\psi f}\cdot\frac{1}{2\lambda_{\psi f}}\tilde{\psi}_f^2\\ & -\underline{\lambda}(Q_s)/\bar{\lambda}(P_s)\cdot\frac{1}{2}E_s^{\mathrm{T}}P_s E_s - K_{Ws}\underline{\lambda}(\Gamma_{ws})\cdot\frac{1}{2}\mathrm{tr}(\tilde{W}_s^{\mathrm{T}}\Gamma_{ws}^{-1}\tilde{W}_s) - K_{\psi s}\lambda_{\psi s}\cdot\frac{1}{2\lambda_{\psi s}}\tilde{\psi}_s^2 + c_2, \end{aligned}$$

where $\bar{\lambda}(\cdot)$ is the maximum eigenvalue. Thus, it satisfies

$$\dot{V} \leqslant -c_1 V + c_2. \tag{55}$$

Hence, the errors including e_f, $\tilde{W}_f$, $\tilde{\psi}_f$, E_s, $\tilde{W}_s$, and $\tilde{\psi}_s$ turn out to be uniformly ultimately bounded. The control law that minimizes the performance index (17) is given by (24), (25), (45) and (47).

Remark 3. The main design work lies in the online learning of the BRFLN and adaptive adjustment of the robust gain. In fact, the control algorithm is not limited to the NGPC. In this paper, the NGPC is utilized mainly because it is a highly efficient algorithm with good performance, which is crucial for the realization of attitudes control system. If some proper nonlinear control methods are combined with the BRFLN, we may apply it to the dynamic systems which don't satisfy the assumptions of NGPC.

5 Simulation results

To verify the control performance of the proposed method, we give an initial point during the NHV's cruise phase (altitude=52 km, velocity=3500 m/s). The flight height means the NHV is in the mesosphere. $\alpha_0 = 1.0°$, $\beta_0 = 3.0°$, $\mu_0 = 2.5°$ and $p_0 = q_0 = r_0 = 0$ rad/s are the initial attitudes. The saturation limiting of δ_e, δ_a and δ_r is $\pm 30°$, while $\pm 15°$ is the limiting of δ_x, δ_y and δ_z.

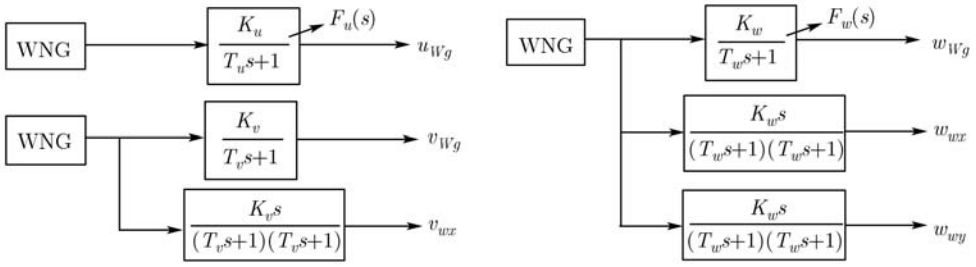

Figure 4 Structure of turbulence generator.

Table 1 Parameters of the BRFLN adaptive control

BRFLNC	Parameters
Fast-loop:	$\delta_f = 0.1$, $\Gamma_{Wf} = 0.35 \cdot I_{13\times 13}$, $K_{Wf} = 0.1$, $\lambda_{\psi f} = 0.01$, $K_{\psi f} = 0.1$
Slow-loop:	$k_p = 6.5$, $k_d = 1.5$, $\delta_s = 0.9$, $\Gamma_{Ws} = 3.5 \cdot I_{13\times 13}$, $K_{Ws} = 5.0$, $\lambda_{\psi s} = 0.1$, $K_{\psi s} = 1.0$

Firstly, suppose that there are $+35\%\sim+55\%$ and $-30\%\sim -50\%$ triangle function uncertainty of the aerodynamic coefficients and aerodynamic moment coefficients respectively. Secondly, adding Dryden turbulence [8] to the average wind velocity can imitate the variable wind field, and it is the atmospheric disturbances exerted on the NHV in section 2. The white noise generator (WNG) enters into shaping filter whose output can simulate the velocity and the gradient of turbulence. We only consider w_{wx}, w_{wy} and v_{wx}, and other gradients are approximately zero. The turbulence generator is shown as Figure 4.

The transfer functions of shaping filters can be seen from [8, 14]. For example,

$$F_u(s) = \sqrt{\frac{2V\sigma_u^2}{L_u}}\frac{1}{s+V/L_u} \text{ and } F_w(s) = \sqrt{\frac{3V\sigma_w^2}{L_w}}\frac{s+V/(\sqrt{3}L_w)}{(s+V/L_w)^2}, \tag{56}$$

where $F_u(s)$ is with longitudinal turbulence and $F_w(s)$ is with vertical one. For the altitude here, the turbulence intensity of moderate turbulence σ_u =6.22 m/s and σ_w =3.25 m/s. Besides, the turbulence scale length L_u =50100 m and L_w= 5200 m [8]. Then, there are variable wind field in the NHV model.

Finally, the disturbance moment upon (16) is defined by

$$\Delta M_C = 6.0\times 10^5(\cos(8t)+0.1)\cdot\cos(7t), (\sin(5t)+0.2), \cos(9t)\cdot\sin(6t))^{\mathrm{T}}.$$

As a result, there exist dynamically changeable Δ_s and Δ_f in (15) and (16).

Figures 5–8 show the attitude control performance of the presented method. The reference outputs are $\alpha_c = 3.0°$, $\beta_c = 1.0°$, and $\mu_c = 4.5°$. In the NGPC design, T_s is set at 0.35 s, and T_f= 0.3 s. The PD+BRFLN adaptive NGPC is applied to the slow-loop system and the BRFLN adaptive NGPC is for the fast-loop system. The three input signals of the BRFLN are expanded into 10-dimension patterns by the third-order B-spline transformations. Initial values of the BRFLN weights and robust gain are set at zero. The sample instant is set at 0.02 s. The controller parameters designed are listed in Table 1.

In Figure 5, the NGPC line denotes control performance of the nominal NGPC. The result shows that there exists large attitude error and the attitude outputs seriously vibrate during most of the simulation time. So the nominal NGPC law cannot satisfy precision and robustness requirements in the presence of large parameter uncertainties and atmospheric disturbances. The FLANC line represents the performance of FLN-based NGPC method. As this figure shows, the outputs still vibrate and the disturbances have not been fully suppressed by the FLN, which is attributed to its little power of learning dynamical nonlinear functions. However, the BRFLN-based NGPC attains a higher precision and better dynamic performance than the FLNAC. Besides, its settling time is within one second, which can satisfy the speediness requirement of the NHV attitude control. Figure 6 shows the control inputs of the NHV. Figure 7 shows changing trends of two adaptive parameters, and it reveals that the BRFLN weight tuning plays a principal role in learning disturbances. In Figure 8, we also provide the approximation performance of the slow-loop disturbances. The nice approximation effect is attained during the simulation time.

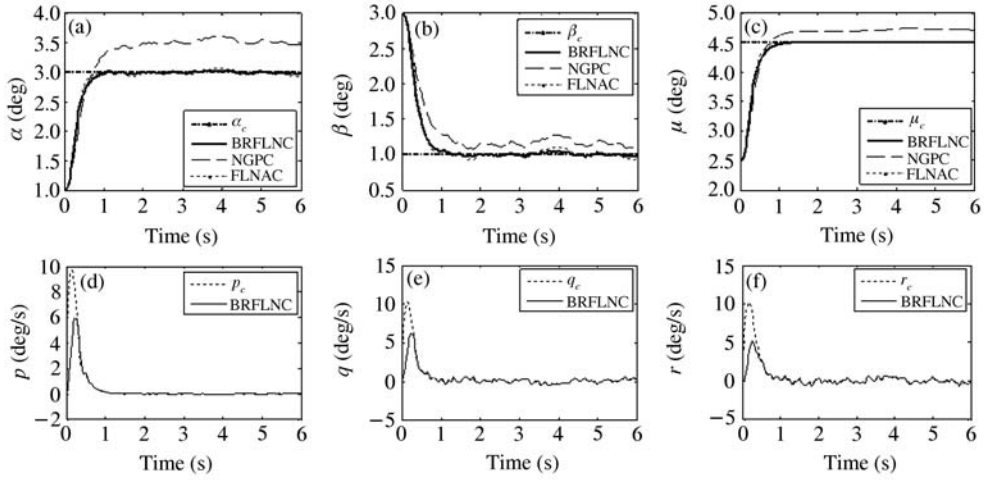

Figure 5 Comparison of attitude control performance. (a) Angle of attack; (b) angle of sideslip; (c) angle of bank; (d) pitch angular rate; (e) roll angular rate; (f) yaw angular rate.

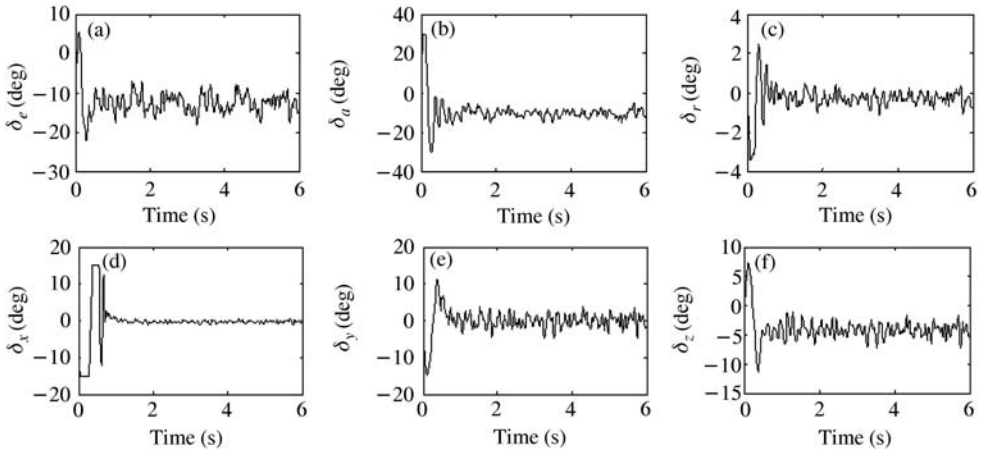

Figure 6 Control surfaces of the NHV. (a) Left elevator; (b) right elevator; (c) rudder; (d) x thrust vector; (e) y thrust vector; (f) z thrust vector.

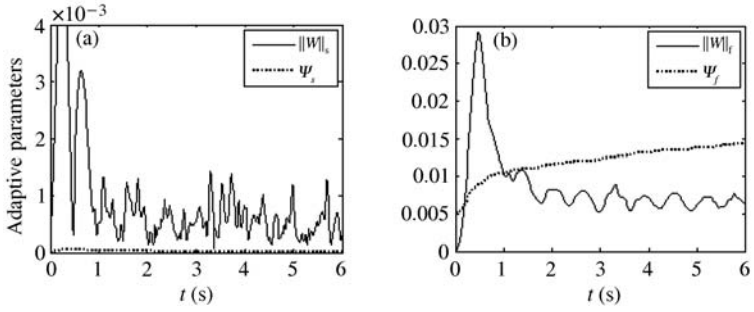

Figure 7 Adaptive parameters of BRFLN-based NGPC. (a) Slow-loop system; (b) fast-loop system.

Remark 4. The NGPC is an efficient predictive control method which does not need the online computing. The BRFLN is a new RNN with simple structure and strong capability of approximating dynamical nonlinear functions. Hence, the combination of the NGPC and the BRFLN can find a compromise between speediness and effectiveness. This method does not require the knowledge about the bounds of uncertainties. The learning process does not need any offline training phase and the initial weights can be selected at random.

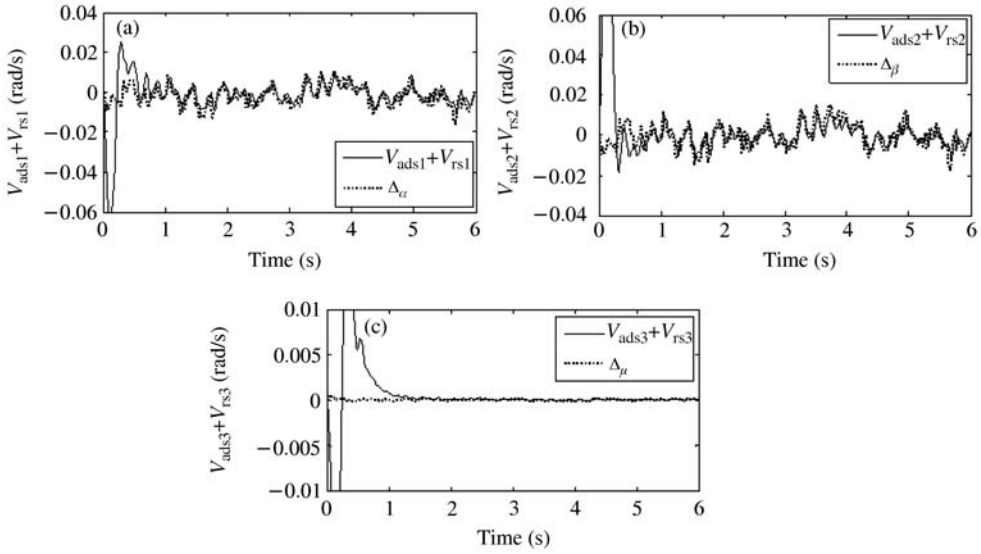

Figure 8 Approximation performance of the slow-loop disturbances. (a) α channel; (b) β channel; (c) μ channel.

6 Conclusions

In this research, we deduces 12 states nonlinear equations of an NHV subjected to variable wind field, so the NHV model is further improved by our work. Aiming at boosting control performance of the NHV with parameter uncertainties and atmospheric disturbances, we propose the BRFLN-based adaptive NGPC method for the attitude control system. Since an NHV in the mesosphere is sensitive to atmospheric disturbances, the BRFLN is designed to approximate fast-loop disturbances, and PD correction BRFLN is utilized to learn slow-loop disturbances. The BRFLN online adaptive law is combined with the NGPC design, and a robust controller with adaptive gain is employed to compensate for the approximation error. Simulation results demonstrate the effectiveness and superiority of the proposed method for the NHV with parameter uncertainties and atmospheric disturbances.

Acknowledgements

This work was supported by the National Natural Science Foundation of China (Grant Nos. 90716028, 60974106).

References

1 Xu H J, Mirmirani M D, Ioannou P A. Adaptive sliding mode control design for a hypersonic flight vehicle. J Guid Control Dynam, 2004, 27: 829–838
2 Poulain F, Piet-Lahanier H, Serre L. Nonlinear control of an air-breathing hypersonic vehicle. In: Proceedings of AIAA International Space Planes and Hypersonic Systems and Technologies Conference, Bremen, AIAA 2009-7290. 2009. 1–14
3 Parker J T, Serrani A, Yurkovich S, et al. Approximate feedback linearization of an air-breathing hypersonic vehicle. In: Proceedings of AIAA Guidance, Navigation, and Control Conference and Exhibit, Keystone, AIAA 2006-6556. 2006. 1–16
4 Fiorentini L, Serrani A. Nonlinear robust adaptive control of flexible air-breathing hypersonic vehicles. J Guid Control Dynam, 2009, 32: 401–415
5 Buschek H, Calise A J. Uncertainty modeling and fixed-order controller design for a hypersonic vehicle model. J Guid Control Dynam, 1997, 20: 42–47
6 Wilcox Z D, MacKunis W, Bhat S, et al. Robust nonlinear control of a hypersonic aircraft in the presence of aerothermoelastic effects. In: Proceedings of 2009 American Control Conference, Lt. Louis, 2009. 2533–2538
7 Du Y L, Wu Q X, Jiang C S, et al. Adaptive functional link network control of near-space vehicle with dynamical uncertainties. J Syst Eng Electr, 2010, 21: 868–876
8 Johnson D L. Terrestrial environment (climatic) criteria guidelines for use in aerospace vehicle development (2008 Revision). NASA/TM-2008–215633. 2008

9 Chen W H, Balance D J, Gawthrop P J. Optimal control of nonlinear systems: a predictive control approach, Automatica, 2003, 39: 633–641
10 Pao Y H. Neural-net computing and intelligent control systems. Int J Control, 1992, 56: 263–289
11 Toh K A, Yau W Y. Fingerprint and speaker verification decisions fusion using functional link artificial neural networks. IEEE Trans Syst Man Cybern -Part C, 2005, 35: 357–370
12 Zhao H Q, Zhang J S. Adaptively combined FIR and functional link artificial neural network equalizer for nonlinear communication channel. IEEE Trans Neural Netw, 2009, 20: 665–674
13 Colgren R, Keshmiri S, Mirmirani M. Nonlinear ten-degree-of-freedom dynamics model of a generic hypersonic vehicle. J Aircraft, 2009, 46: 800–813
14 Xiao Y L, Jin C J. Flight Principle in Atmospheric Disturbance (in Chinese). Beijing: Defense Industry Press, 1993. 73–78
15 Isidori A. Nonlinear Control Systems (in Chinese). 3rd ed. Beijing: Publishing House of Electronics Industry, 1995. 172–173
16 Wu B, Wu K, Lü J H. A novel compensation-based recurrent fuzzy neural network and its learning algorithm. Sci China Ser F-Inf Sci, 2009, 52: 41–51
17 Samadi S, Ahmad M O, Swamy M N S. Characterization of B-spline digital filters. IEEE Trans Circ Syst, 2004, 51: 808–816
18 Polycarpou M M. Stable adaptive neural control scheme for nonlinear systems. IEEE Trans Automat Control, 1996, 41: 447–451